AMERICAN SCIENTIFIC PUBLISHERS

Reviews in Nanoscience and Nanotechnology
Vol. 3, pp. 77–87, 2014
(www.aspbs.com/rnn)

Design and Characterization of Photonic Crystal Membrane Reflector Based Vertical Cavity Surface Emitting Lasers on Silicon

Deyin Zhao[1], Hongjun Yang[1,3], Jung-Hun Seo[2], Zhenqiang Ma[2], and Weidong Zhou[1,*]

[1]*Department of Electrical Engineering, NanoFAB Center, University of Texas at Arlington, TX 76019, USA*
[2]*Department of Electrical and Computer Engineering, University of Wisconsin-Madison, WI 53706, USA*
[3]*Semerane, Inc., 202 East Border Street, Suite 149, Arlington, Texas 76010, USA*

Silicon-based light source integrated in photonics and electronics circuits with low cost and high efficiency has been an attractive research and development direction worldwide. The hybrid approach, in which silicon is integrated with a III–V gain medium, is an effective way. Using a transfer-printing and multilayer semiconductor nanomembrane stacking process, an optically pumped surface-emitting laser on silicon is realized, which is sandwiched between two single-layer silicon photonic crystal Fano resonance membrane reflectors (MRs). Here we review the design and characteristics of this Si based laser cavity, including the principle, design and phase properties of the membrane reflector, the cavity design and mode analysis, and experimental demonstration of the MR reflections as well as performance and the lasing behavior.

KEYWORDS: Vertical Cavity Surface Emitting Laser, Si Nanomembrane Reflector, Photonic Crystal, Fano Resonance.

CONTENTS

1. INTRODUCTION

Among various types of lasers, vertical-cavity surface-emitting lasers (VCSELs) are the one of the popular type for a wide range of applications which require low threshold, high wall plug-efficiency, high modulation speed, and low cost large volume production.[1–5] Traditional VCSELs consist of two distributed Bragg reflectors (DBRs) as top and bottom mirrors which provide the optical feedback to form the cavity, as shown in Figure 1. Due to the very short gain lengths in the center of VCSELs cavity, a very high reflectivity (> 99%) is always required in the DBRs to lower the lasing threshold.[2,6] DBRs are mostly fabricated by using monolithically grown technology and the constrained index difference of the alternating materials is small. Therefore, the DBRs are typically very thick. While the DBR fabrication technology is mature for GaAs-based VCSELs, it is still a big challenge for InP-based longer wavelength VCSELs, due to the lack of the lattice-matched alternative materials with large index contrast.[7]

Single thin layer structures with one-dimensional (1D) subwavelength grating (SWG) and 2D photonic crystal (PC) patterns can also offer very high reflectivity,[8–12] which can replace the DBRs of traditional VCSELs. In 2007, electrically and optically pumped VCSELs have been reported by replacing the top DBR with 1D SWG reflector.[13,14] whose cavity structures are shown in Figures 2(a) and (b) respectively. In these VCSELs, the growth method is involved to form the cavity and the devices are processed on the III–V native substrates. In 2012, by replacing both top and bottom DBRs, optically-pumped VCSELs on Si were realized by using two different techniques.[15,16] Utilizing the III–V/SiO_2 molecular bonding processes and amorphous Si deposition processes, Viktorovitch et al. formed the VCSEL cavity with two 1D Si membrane grating reflectors shown in Figure 3(a). By employing transfer printing technology, we reported optically pumped MR-VCSELs on Si by sandwiching an InGaAsP QW active cavity in

*Author to whom correspondence should be addressed.
Email: wzhou@uta.edu
Received: 13 April 2014
Accepted: 27 May 2014

between two 2D photonic crystal Fano resonance membrane reflectors (MRs), shown in Figure 3(b).

Due to different mechanisms, the Fano resonance PCMRs have different phase and energy penetration characteristics.[17–20] Additionally, in the MR-VCSEL cavity, two MRs also act as two couplers which can excite the waveguide (WG) modes in QW layer if the coupling condition is satisfied.[21,22] The WGs will lead to an additional lateral loss if it overlaps with the cavity mode. These unique characteristics of MRs are very important and should be taken into consideration carefully in the MR-VCSEL cavity design.

Deyin Zhao is a Researcher Associate at Nano Photonics Lab, Department of Electrical Engineering at University of Texas at Arlington (UTA) since August 2008. He received his Ph.D. degree in 2008 from Shanghai Institute of Microsystem and Information Technology, China. Dr. Zhao's expertise are theoretical design, numerical simulation, characterization and analysis on various optical and optoelectronic devices with conventional and photonic crystal nanostructures, such as light sources and VCSELs, dielectric reflector, filter, modulators, photodetector, sensor, solar cells, etc. His research interests are seeking novel optical designs and developing their practical applications in optical communication, biology, environment, and other interdisciplines.

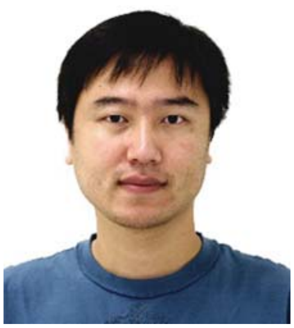

Hongjun Yang received his Ph.D. in Electrical Engineering from University of Texas at Arlington in 2010. He joined Semerane Inc. as a senior research scientist after graduation, then has been prompted to the director of engineering. He delivered various active research projects in the areas of photonic crystal infrared photodetectors, silicon based detectors, sources, and modulators, cost effective solar cells, VCSELs, etc., based on photonic crystals, semiconductor nanomembranes, quantum dots, and other nanoscale structure. He has authored and co-authored 50+ papers including peer-reviewed journal articles, invited and contributed conference papers.

Jung-Hun Seo received the B.S. and M.S. degree in electronics and electrical engineering from Korea University, Seoul, Republic of Korea, in 2006, 2008, respectively. From 2009, he is currently working toward the Ph.D. candidate in electrical and computer engineering at University of Wisconsin-Madison, USA. He's authored and coauthored more than 35 peer-reviewed papers. His current research interests are fast flexible electronics and wide bandgap HBTs.

Zhenqiang Ma, a Lynn H. Matthias Professor in Engineering and Vilas Distinguished Achievement Professor, received the B.S. degree in applied physics and the B.E. degree in electrical engineering from Tsinghua University, Beijing, China, both in 1991, and the M.S./M.S.E. degree in nuclear science/electrical engineering and the Ph.D. degree in electrical engineering from the University of Michigan, Ann Arbor, both in 1997 and 2001, respectively. Since 2002, he has been with Department of Electrical and Computer Engineering, University of Wisconsin, Madison, as a Professor. In 2008, he received Presidential Early Career Award for Scientists and Engineers (PECASE) and DARPA Young Faculty Award He is the author or coauthor of more than 120 peer reviewed papers and book chapters. His current research interests include semiconductor materials, processing and heterogeneous integration, semiconductor device physics and technologies, high-speed electronic and optoelectronic devices, CMOS integrations with lasers and with micro-/nano electromechanical systems (MEMS/NEMS), nanophotonics based on transferable semiconductor membranes, high-speed flextronics, nanoscale semiconductor devices, unconventional multispectral imaging, photovoltaics, isotope betavoltaics, and high frequency RF integrated circuits.

Weidong Zhou is a professor of Electrical Engineering at University of Texas at Arlington. He obtained his B.S. and M.E. degrees from Tsinghua University, Beijing, China, in 1993 and 1996, respectively. He obtained his Ph.D. degree in Electrical Engineering from University of Michigan, Ann Arbor, in 2001. From 2001–2004, he worked as a lead engineer at CIENA corporation, working on active photonic devices for optical fiber communication systems. Dr. Zhou's research interests include nanophtoonics and optoelectronic devices, based on photonic crystals and metamaterials, with focus on lasers for silicon photonics, optical cavities and optical coatings for detectors and solar cells. Dr. Zhou has authored and co-authored over 230 journal publications and conference presentations, including ~40 invited conference talks.

Figure 4 shows the sketch of the MR-VCSEL cavity which consists of a III–V InGaAsP quantum well (QW) disk, sandwiched in between two single-layer Si photonic crystal (PC) Fano resonance membrane reflectors (Si-MRs). Two low index buffer layers (SiO_2, layers t_2 and t_4) are inserted to ensure proper index contrast to the top and bottom Si-MRs. The complete MR-VCSEL cavity (t_1 to t_5) is built on the top of a silicon-on-insulator (SOI) substrate with SiO_2 buried oxide (BOX) layer thickness of t_0. In order to achieve lasing with low threshold in such a cavity, it is highly desirable to design MR-VCSEL cavity with the following characteristics: (a) Both top and bottom MRs should have broadband reflection bands, with reflections greater than 99%; (b) The cavity should be designed such that the cavity mode is spectrally separated from the waveguide modes; (c) The cavity mode should match with QW emission peak spectrally with or without spectral detuning; and (d) The cavity mode should have an optimal field distribution spatially matched with QW active region for high confinement factors and low lasing thresholds.

In this paper, we report a systematic review on designs and characteristics of MR and MR-VCSEL cavity. First, we discuss the MR reflection principle, design and phase properties. Next, we present MR-VCSELs cavity design and cavity mode analysis. In the fourth section, we experimentally demonstrate the MR reflections and the lasing behavior. The conclusion and the further applications of the MR-VCSEL are discussed at the end.

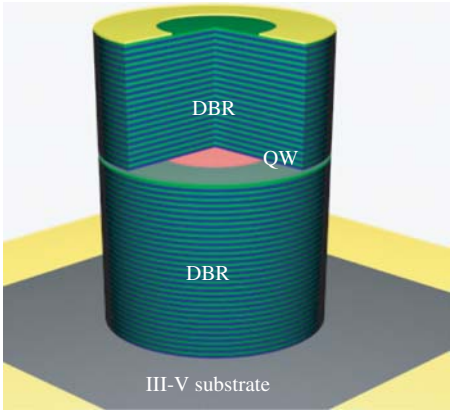

Fig. 1. Schematic of a traditional DBR based VCSEL with top and bottom DBRs grown on III–V substrate.

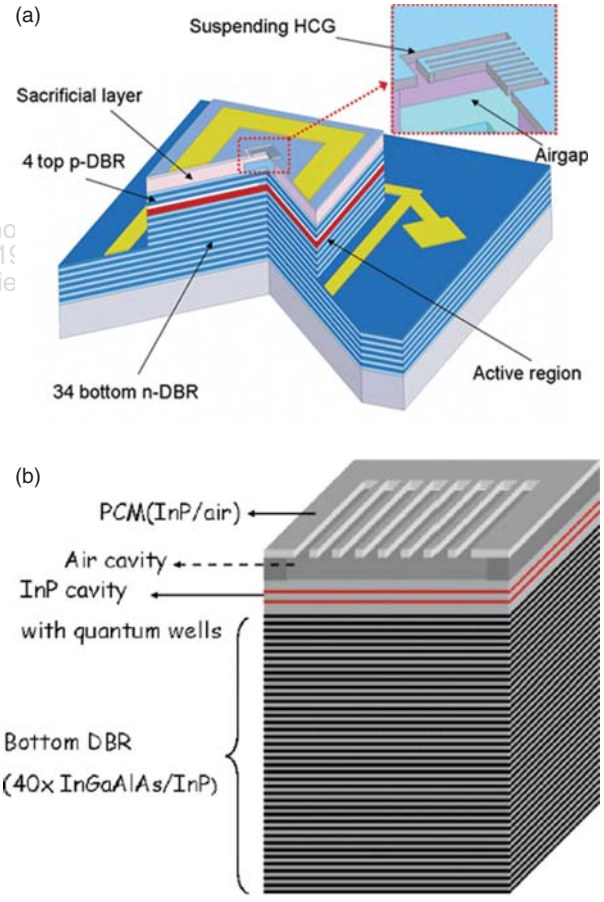

Fig. 2. VCSELs with top MR/bottom DBR: (a) electrically pump, and GaAs 1D SWG reflector grown on GaAs substrate; and (b) optically pump, and InP 1D SWG grown on InP substrate. Reproduced with permissions from [13, 14], M. C. Y. Huang, et al., A surface-emitting laser incorporating a high-index-contrast subwavelength grating 1, 119 **(2007)**, *Nat. Photonics* 1, 297 **(2007)**. © 2007, Nature Publishing Group. S. Boutami, et al., Compact and polarization controlled 1.55 μm vertical-cavity surface-emitting laser using single-layer photonic crystal mirror. *Appl. Phys. Lett.* 91, 13 **(2007)**. © 2007, AIP.

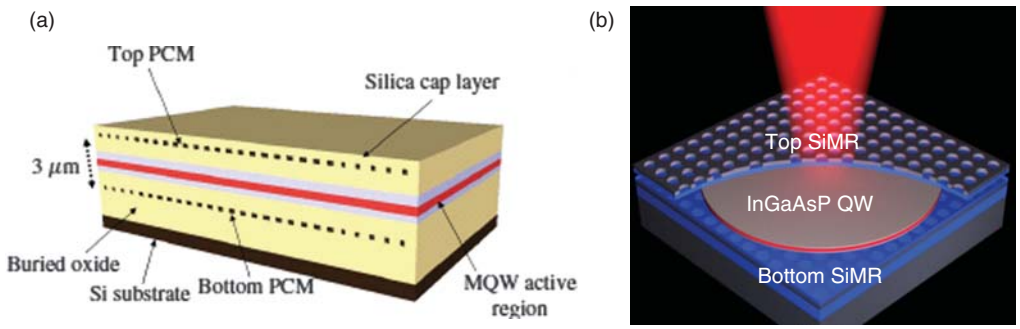

Fig. 3. Schematics of VCSELs with (a) double SWGs and (b) double 2D PC MRs. Reproduced with permission from [15, 16] C. Sciancalepore, et al., CMOS-compatible ultra-compact 1.55-μm emitting VCSELs using double photonic crystal mirrors. *Photonics Technology Letters, IEEE* 24, 455 **(2012)**. © 2012, IEEE. H. Yang, et al., Transfer printing stacked nanomembrane lasers on silicon. *Nat. Photonics* 25, 658 **(2012)**. © 2012, Macmillan Publishers Limited.

2. SI MR REFLECTOR

2.1. Principle and Design Towards Broadband and High Reflectance

Single layer nanomembrane with 1D or 2D photonic crystal pattern can be functioned as broad band reflectors, whose high reflection mechanism originate from the Fano- or guided-resonances effect and is completely different from the traditional DBR.[23–25] The spectral bandwidth and reflection properties of DBRs have been well studied.[19] The high reflectivity attributes to the multiple reflections with constructive interference among these reflected waves by each thin layer inside of DBR. And the larger index difference gives rise to a broader reflection band. For 1D SWG and 2D PC mirrors, the reflection mechanism comes from Fano or Guided mode resonance effect and the destructive interference effect. In Ref., Magnusson et al.[24] attributed the broadband reflection of SWG to the in-plane guided-mode excitation based on phase matching conditions. The wave then reradiates at one edge with a zero phase difference and at another edge with a π phase difference. The broad reflection spectral band originates from the cooperating of the several adjacent guided mode resonances. As shown in Figure 5(a), in a Si-based SWG design with target reflection band over 1.45–2.0 μm for TM polarization, the very broadband reflection bandwidth of 520 nm for 99% reflectionis supported by a blend of three guided mode resonances (transmission dips) located inside this band. On the other hand, in Ref. [25] Karagodsky et al. presented an analytic analysis on the ultra-high reflectivity of subwavelength high contrast grating reflectors based on double grating modes model. The double modes exhibit perfect cancellation at the output plane of SWG, i.e., π phase difference or completely destructive interference. As clearly shown in Figure 5(b), the average E-fields of the first two grating modes are plotted with their phase difference. At the points of 100% reflectivity the modes have anti-phase with equal intensities, which means that perfect cancellation occurs. If two such 100% reflectivity points are located at close spectral vicinity, a broad-band of high reflectivity is achieved.

According to the principle of MRs, to achieve broadband high reflection, the first thing is to choose the structure parameters, including membrane thickness "t," PC lattice "a," air hole radius "r," and substrate index "n," which can support Fano/guided-mode resonances in the target spectral band, then one can tune the parameter to find optimized one. Sang et al. presented a systematical design guideline in a Ref. [26]. Using the trial-and-error approaches based on the complete 3D computational tools, such as RCWA and FDTD techniques, the different designs for high Q filters (narrow band reflector) and broadband MRs can be done. It was found that the Q factor (spectral line width) can be controlled by varying the radius once the proper membrane thickness is found. Very small r/a values ($\sim$0.1) favor high Q filter design and large r/a values (0.28–0.49) favor broadband reflector design. Other design parameters include the lattice structure and the air hole shape, the surrounding buffer, and the effective indices inside PC pattern region, etc. From the previous works,[9, 27–29] the thickness of 340 nm is found to bea better parameter of a single crystalline Si

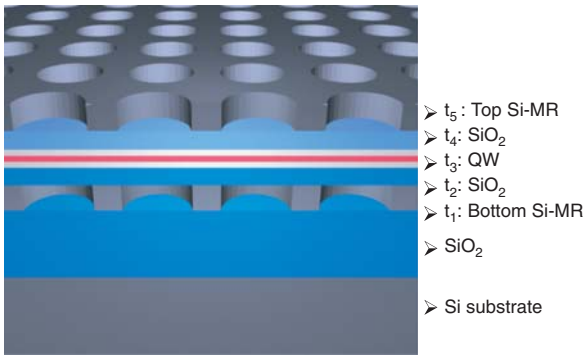

Fig. 4. Membrane reflector VCSEL (MR-VCSEL) schematic of a complete MR-VCSEL cut-out view: an InGaAsP QW sandwiched in between two single layer Si Fano resonance photonic crystal membrane reflectors (SiMRs), stacked on a Si substrate. Low index SiO_2 buffer layers are inserted to ensure high reflection of MRs. The whole cavity consists of five layers (t_1–t_5). Reproduced with permission from [21], D. Zhao, et al., Design of photonic crystal membrane reflector based VCSELs. *IEEE Photonics Journal* 4, 2169 **(2012)**. © 2012, IEEE.

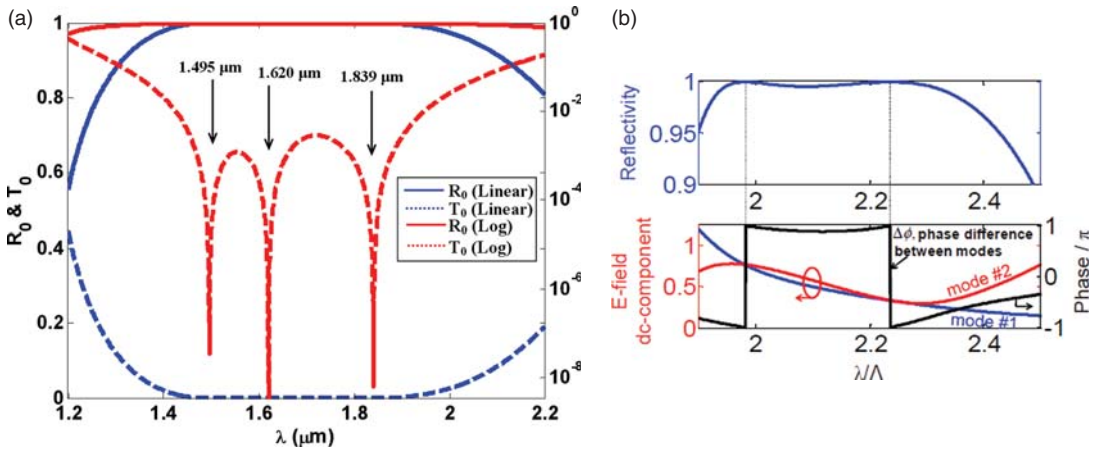

Fig. 5. (a) Physical basis for broadband reflection in 1D gratings: Zero-order reflectance and transmittance spectra of broadband reflectors operating in (a) TM polarizations. For clarity, the spectra are plotted on both linear and logarithmic scales. Reproduced with permission from [24], R. Magnusson and M. Shokooh-Saremi, Physical basis for wideband resonant reflectors. *Opt. Express* 16, 3456 **(2008)**. © 2008, OSA. (b) Double-mode solution exhibits perfect cancellation at the SWG output plane leading to 100% reflectivity. At the wavelengths of 100% reflectivity both modes have the same magnitude and opposite phases π. Reproduced with permission from [25], V. Karagodsky, et al., Theoretical analysis of subwavelength high contrast grating reflectors. *Opt. Express* 18, 16973 **(2010)**. © 2010, OSA.

nanomembrane with index $n = 3.48$ to design MRs with broad band spectral and high reflection in the optical communication band around 1550 nm. Here we present two good group designs with medium ($r = 0.3a$) and larger ($r = 0.45a$) air hole for top MR (on glass substrate, $a =$ 1010 nm) and bottom MR (on SOI, $a = 880$ nm, BOX thickness t_0=2μm), as shown in Figures 6(a) and (b), respectively. For the bottom MR, another layer of SiO_2 low index buffer layer (t_2) is also incorporated in the design, as part of the complete MR-VCSEL as shown in Figure 4. During SiO_2 deposition, air hole will be partially filled. So the effective index inside air hole region (n_f) should be considered. According to earlier theoretical and experiment results[28] the effective index for the air hole region (n_f) is about 1.2 for Si-MRs with larger air hole design ($r/a > 0.4$). One can see the bottom MR reflection band cover from 1300 to 1600 nm with $R > 99\%$. Through adjusting main parameters, (t, a, r), MRs for different band range can be obtained. Qiang et al. reported more designs forMRs on SOI based on the control of vertical confinement with controlled refractive index for the buffer layers below and above the MR layer.[28]

Experimentally, Boutami et al.[30] reported demonstration of 2D PCS based MRs with controlled polarization and broad reflection band of 200 nm at 1550 nm wavelength region. Later, Yang et al. reported detailed experimental investigations with index tuning range over 50 nm for both blue and red shifts, by controlling the buffer oxide index below with controlled etching and the index above with the controlled oxide deposition.[27]

2.2. Phase, Energy and Phase Penetration Properties in Membrane Reflectors

Under surface-normal incidence, DBR, 1D SWG, and 2D PCS reflectors can all exhibit similar reflection properties with extremely high reflection and broad reflection spectral band. However, the different reflection mechanisms lead to different phase and penetration properties.

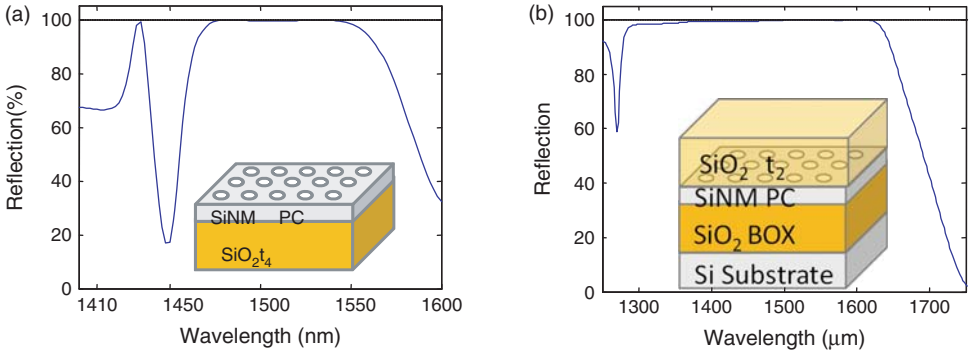

Fig. 6. Simulated reflection of top and bottom MR. (a), Bottom MR based on SOI structure with SiO_2 deposition as buffer layer with thickness t_2~400 nm. (b), Top MR transferred on another SiO_2 buffer layer with thickness t_4~400 nm. Reproduced with permission from [21], D. Zhao, et al., Design of photonic crystal membrane reflector based VCSELs. *IEEE Photonics Journal* 4, 2169 **(2012)**. © 2012, IEEE.

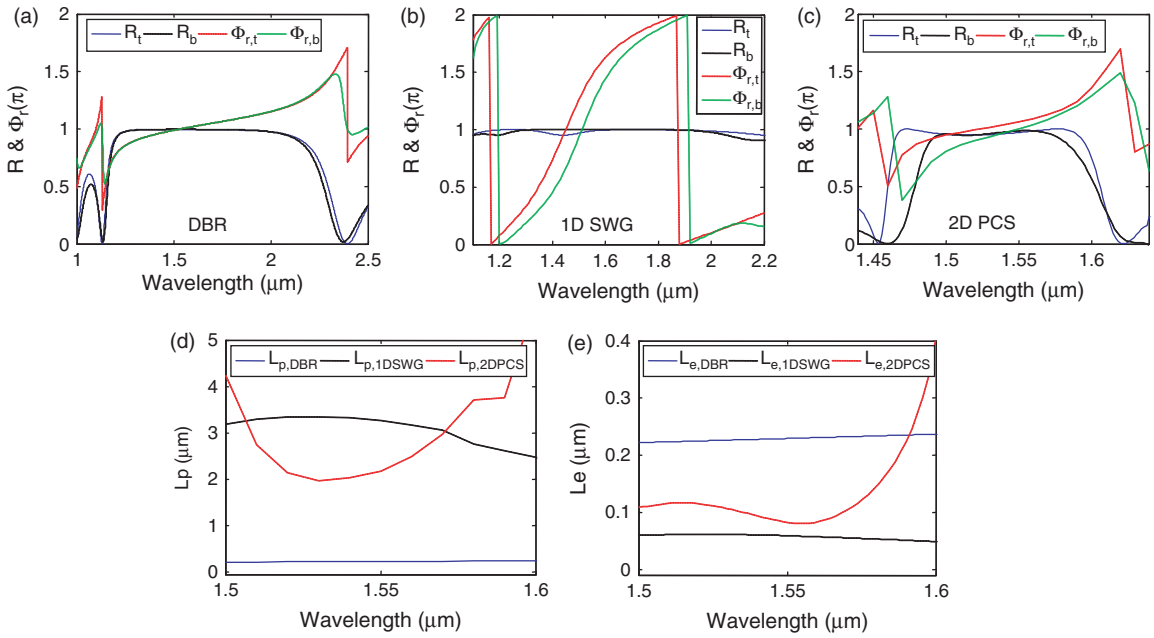

Fig. 7. (a)–(c) Simulated reflection and reflection phase change of three types of reflectors; (d) calculated phase penetration depths for three types of reflectors; and (e) the energy penetration depths for three types of reflectors. Reproduced with permission from [17], D. Y. Zhao, et al., Field penetrations in photonic crystal fano reflectors. *Opt. Express* 18, 14152 **(2010)**. © 2010.

In Ref. [31] the authors reported the phase discontinuity Φr and the energy penetration depth (Le) according to the mode spacing in the Fabry-Perot (FP) cavity. In 2009, the in-plane optical property of 2D PCS was reported by Sauvan et al.[20] With fully vectorial calculations, in heterostructure mirrors, the penetration length associated with the delay is much larger than the characteristic damping length of the energy distribution inside the mirror. This amazing property evidences that these two characteristic lengths are not necessarily correlated. Consequently, the usual trade-off between short damping lengths and large penetration lengths that is encountered in classical DBRs can be overcome with carefully designed PC structures. Later Zhao et al.[17] investigated in more details the phase and energy penetration depths, and field distributions of 1D SWG and 2D PCS reflectors, as shown in Figure 7. Figures 7(a)–(c) show the reflection phase change of DBR, 1D SWG and 2D PCS, respectively. One can see Φ_r of 1D SWG and 2D PCS reflectors rapidly vary in the high reflection ($R > 0.95$) spectral band, much faster than those of DBRs.

In dielectric mirrors, the reflection is not an instantaneous process. It includes a reflection time delay (τ) or phase penetration depth (Lp) and energy storage in the mirrors. The phase penetration depth (Lp) is always directly related to the reflection phase shift Φr, so Lp of 1D SWG and 2D PCS are much larger than DBR,as shown in Figure 7(d). The energy penetration depth (Le) is related the energy storage. Figure 7(e) shows Le comparison of these three mirrors. One can see Le of 1D SWG and 2D PCS are much smaller than DBR. In addition, for 1D SWG and 2D PCS, Lp is much larger than Le, while Lp and Le of DBR are close to each other. Therefore, comparing to the DBR reflectors, these new types of single layer ultra-compact broadband reflectors can have more complicated larger phase delays and smaller energy penetration properties, which can be engineered via dispersion engineering for large spectral dependent phase delays, and ultra-small energy penetration depths. This phase information is important and helpful in the following cavity design.

3. MR-VCSEL DESIGN

Once two good MRs with high reflectivity and broader overlapped spectral band are obtained, a multi-layer Si-MR/QW/Si-MR MR-VCSEL cavity can be build up. Here, we need to decide the cavity resonant (longitude) mode by selecting a suitable cavity length, i.e., the thickness of the buffer layers between Si-MR and QW. Figure 8(a) shows the reflection spectrum (blue line) of one designed MR-VCSEL cavity with $t_0 = 2\ \mu$m, $t_1 = t_5 = 340$ nm, $t_2 = t_4 = 400$ nm, $t_3 = 465$ nm, $a = 860$ nm, $r_t = 0.46a$ and $r_b = 0.45a$. The resonant cavity mode appears at 1478 nm. To make the field distribution more symmetric inside cavity, another SiO_2 layer with $t_6 = 400$ nm or thicker is assumed to be deposited on the top of MR-VCSEL and $n_f = 1.2$ is also considered. To further confirm this cavity mode, the phase resonant condition (total phase change of one round-trip in cavity is equal to integer times of 2π) is also calculated according the reflection phase change (ϕ) of the top and bottom MR, which is plotted as red dotted line in Figure 8(a). One can find the mode located at

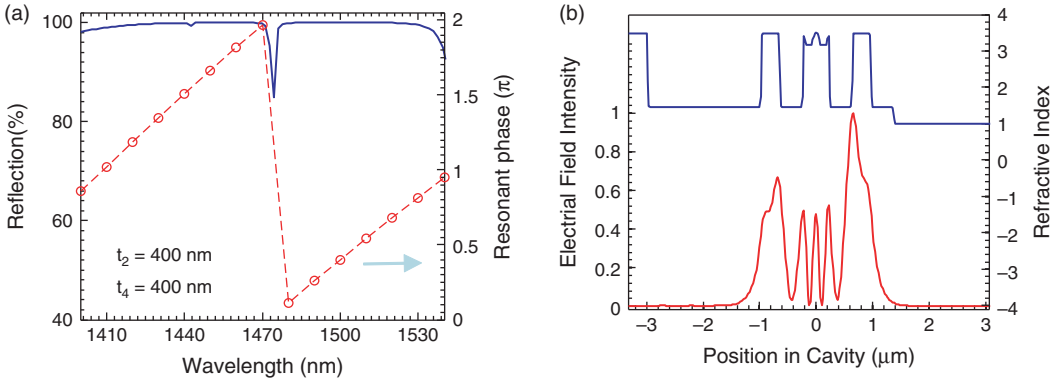

Fig. 8. Characteristics of designed MR-VCSEL cavity. (a), Calculated cavity resonance mode based on cavity reflection and phase resonant condition. (b), Field distribution of cavity mode. Reproduced with permission from [21], D. Zhao, et al., Design of photonic crystal membrane reflector based VCSELs. *IEEE Photonics Journal* 4, 2169 **(2012)**. © 2012, IEEE.

1478 nm has a m·2π phase change, which means 1478 nm is a real cavity mode.

By employing FDTD, a short temporal Gaussian pulse is used to excite the cavity modes and the quality factor of the cavity mode 1478 nm is calculated to be 4300 according to $Q = Re(\omega)/-2\cdot Im(\omega)$.[32] Then a longer temporal Gaussian pulse is used to excite the single cavity mode and the stable field is recorded. The E-field distribution is demonstrated in Figure 8(b) with red line, where the cavity index profile is also plotted with blue line. One of E-field peak is located at QW well region and the calculated confinement factor is about $\Gamma = 5.6\%$.

Another design concern should be taken care, i.e., separating the lasing cavity modes from the waveguide modes within the QW layer as mentioned in a Ref. [21]. Despite the relatively large field concentration in Si-MR layer, the lasing mode field confinement factor is 5.6% for MR-VCSELs, which is comparable to DBR-based VCSELs.

4. MR-VCSEL OPTICAL CHARACTERISTICS

4.1. MR Reflection

Using the designed Si-MR parameters discussed in the previous section, the top MR was first fabricated on SOI

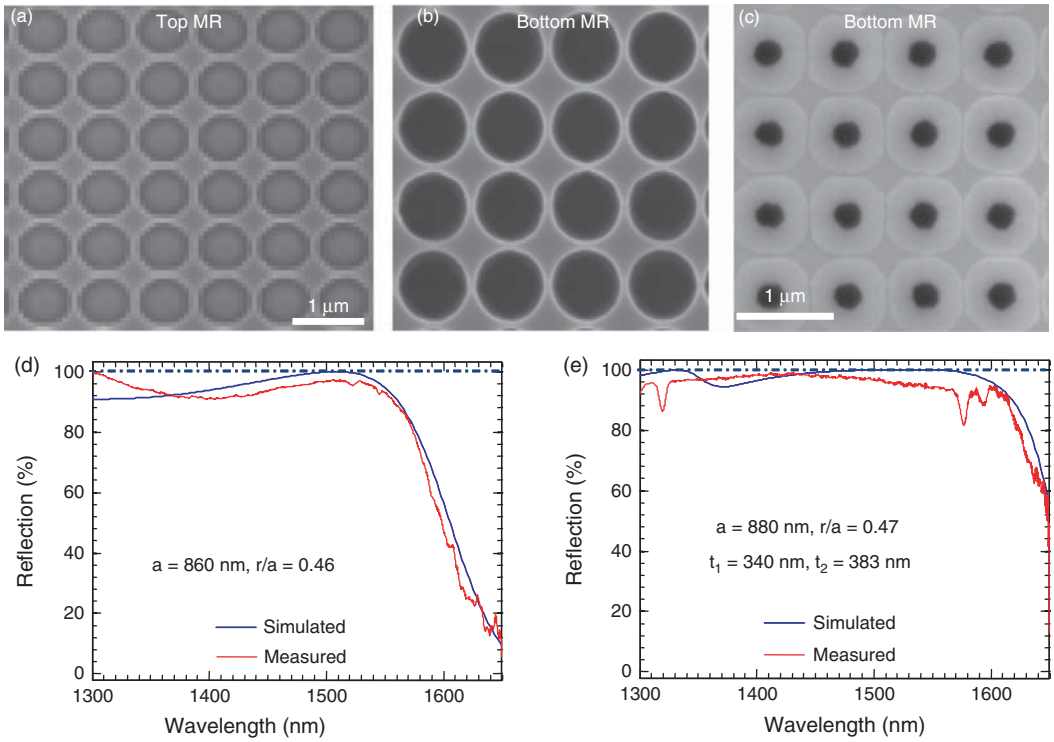

Fig. 9. (a)–(c), SEM images of membrane reflectors (MRs). (d) and (e) the measured and simulated reflection of top and bottom MRs. Reproduced with permission from [16], H. Yang, et al., Transfer printing stacked nanomembrane lasers on silicon. *Nat. Photonics* 25, 658 **(2012)**. © 2012, Macmillan Publishers Limited.

and then transferred onto a glass substrate employing the elastomeric stamp based transfer printing process.[16] Figure 9(a) is the scanning electron micrograph (SEM) image of the transferred top MR on glass substrate with $a = 860$ nm and $r/a = 0.46$. The bottom SiMR with $a = 860$ nm and $r/a = 0.45$ is directly fabricated on a SOI substrate and followed by a deposition of a thin SiO_2 film on its top, with SiO_2 layer thickness $t_2 \sim 383$ nm, to work as a cavity buffer layer. SEM images of two cases, before and after the top SiO_2 deposition, are shown in Figures 9(b) and (c), respectively. Due to the large r/a, air holes become smaller and not completely sealed by this thin SiO_2 deposition, which means SiO_2 is partially filled into the air holes and is considered in our designs by using an effective index in the air hole region.

The reflections of these two MRs are measured under normal incidence using a slightly focused white light beam and normalized with gold mirror. The simulation and measurement results of the top and the bottom MRs are plotted together in Figures 9(d) and (e). The reflectors designed to have peak reflection values $> 99\%$, with wide reflection bands. Also, the measured and simulated reflections are matched well. It should be noted that the small dip at the edge of high reflection band comes from the non-ideal normal incidence, i.e., the slightly focused beam includes a small partial of oblique incident light around the beam edge.

4.2. Half Cavity Characteristics

The InGaAsP QW disks are transferred onto the bottom Si-MR after the substrate removel. Figures 10(a) and (b) show the micrograph and SEM image of this half cavity without top MR. Some QW disks are transferred onto a patterned bottom Si-MR region, while the others are laid onto the unpatterned Si region. The diameter D of these QW disks (i.e., the active area of the MR-VCSELs) is 100 μm. The PL performances of QW disks on-MR and off-MR were tested under various temperature (T) from 10 K to 300 K using a continuous wave (c.w.) green laser. Figure 10(c) shows the PL spectra of the disks on MR (solid lines) and off-MR (dashed lines) at different T, where the bottom MR reflection at 300 K is also plotted together as a reference. As T increases, the common PL features can be found, PL spectral shift towards longer wavelength, intensity reduces, and spectral becomes broader. In Figure 10(d), the linearly fitted PL peak location indicates PL peaks are red-shifted with a rate of 0.43 nm/K. Due to the high reflection of bottom Si-MR, the PL intensity is much enhanced. Shown in Figure 10(d) is the PL peak intensity enhancement factor as a function of T. For $T < 150$ K, PL of QW disk on-MR is enhanced by 3 times comparing with off-MR, and

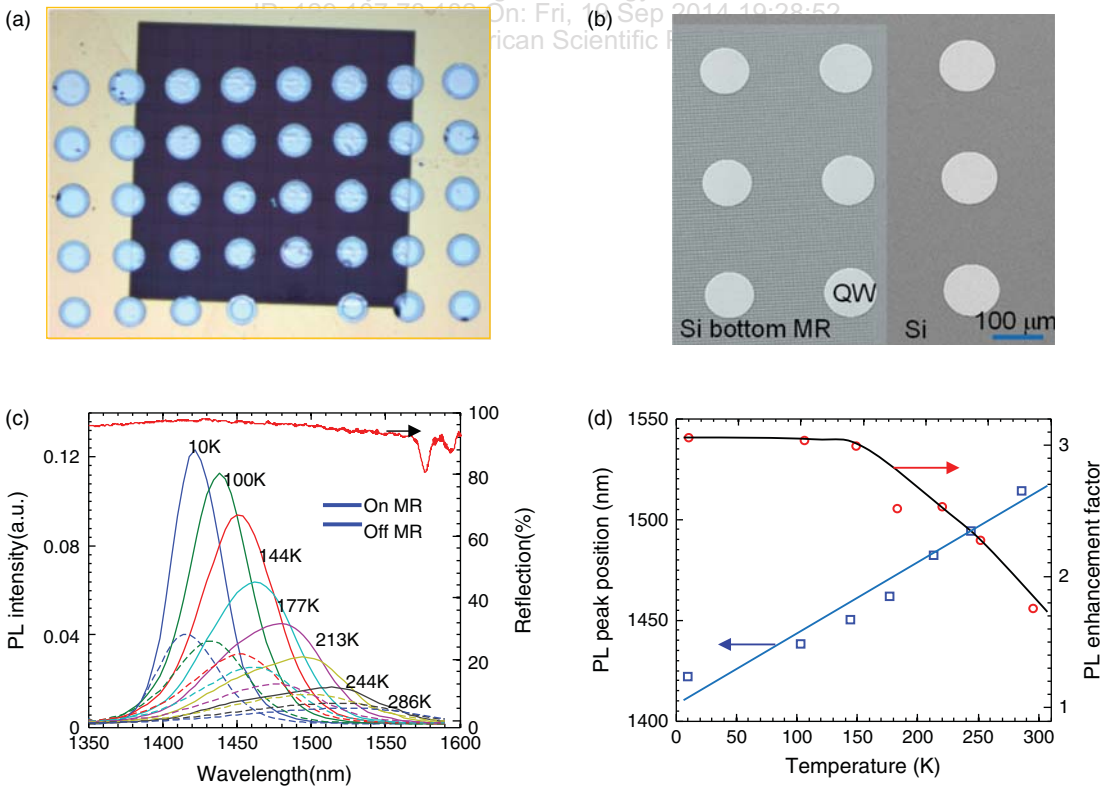

Fig. 10. (a) and (b) Micrograph and SEM images of half cavity (QW on bottom MR); Reproduced with permission from [16], H. Yang, et al., Transfer printing stacked nanomembrane lasers on silicon. *Nat. Photonics* 25, 658 (**2012**). © 2012, Macmillan Publishers Limited. (c) the PL spectral of the QW disk on and off-MR as function of temperature, where the bottom MR reflection is also plotted with red line; (d) PL peak location and intensity enhancement factor versus T.

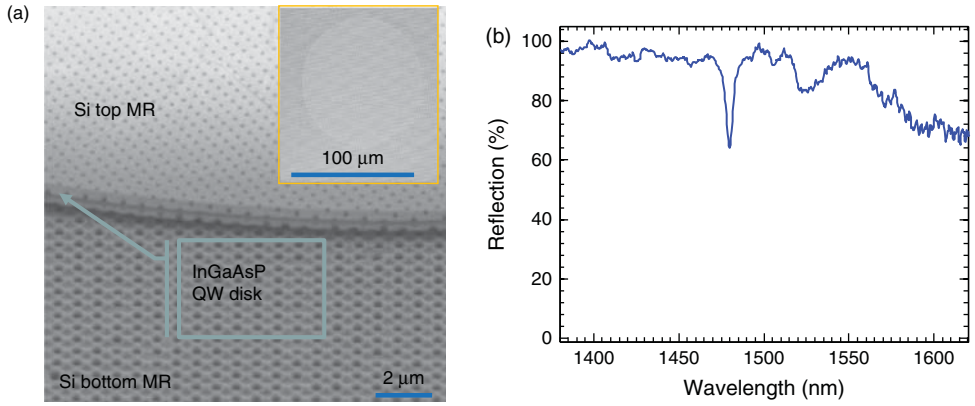

Fig. 11. (a) SEM image of the complete MR-VCSEL; Reproduced with permission from [16], H. Yang, et al., Transfer printing stacked nanomembrane lasers on silicon. *Nat. Photonics* 25, 658 **(2012)**. © 2012, Macmillan Publishers Limited. (b) The measured cavity reflections.

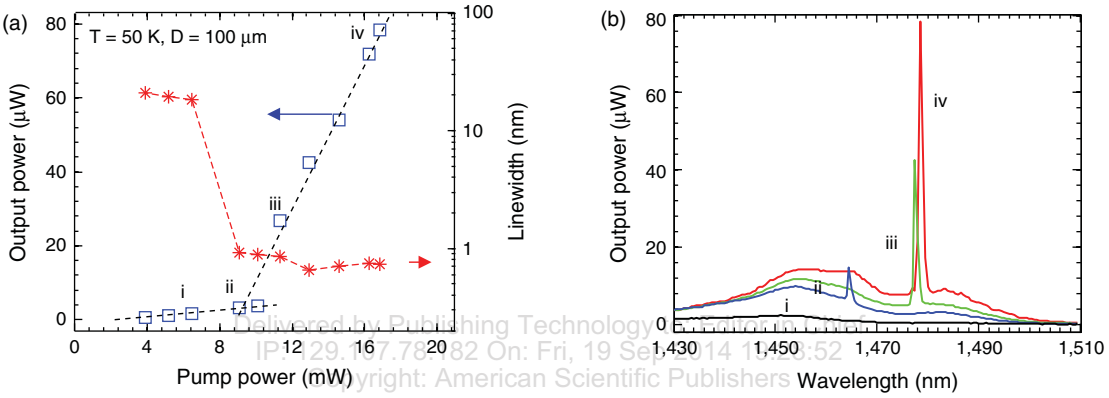

Fig. 12. (a), The L–L plot (light output for different pump powers) and the corresponding spectral linewidths at $T = 50$ K; (b) The measured spectral outputs for pump powers below, at, and above thresholds. Reproduced with permission from [16], H. Yang, et al., Transfer printing stacked nanomembrane lasers on silicon. *Nat. Photonics* 25, 658 **(2012)**. © 2012, Macmillan Publishers Limited.

when $T > 150$ K, the PL enhancement reduces down to 1.8 times because MR reflection at longer wavelength range becomes lower.

4.3. Lasing Behaviors

A complete MR-VCSEL structure is shown in Figure 11(a), where both the top and the bottom Si-MRs are visible. The inset shows a single QW disk underneath the top Si-MR layer. Figure 11(b) is the cavity reflection measured with white light source at normal incidence. One can find the cavity mode is at around 1478 nm, which matches the cavity mode design.

The MR-VCSEL device was tested under PL setup using quasi-continuous wave (c.w.) 532 nm laser pumping

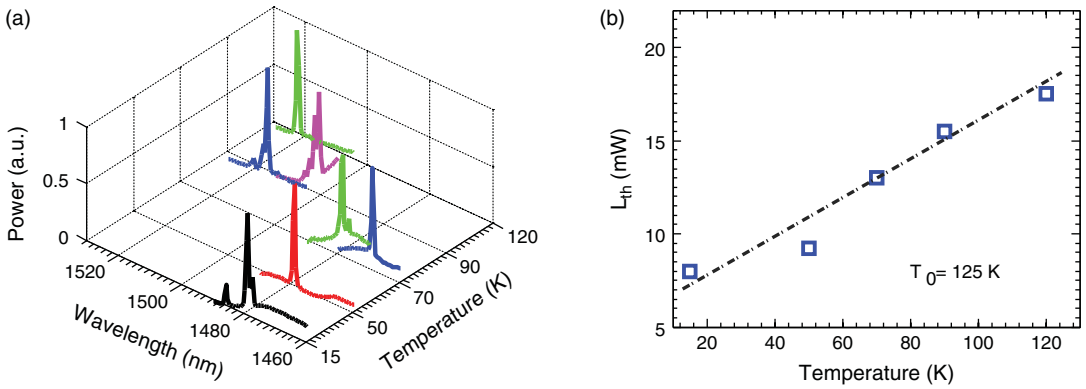

Fig. 13. (a) Measured lasing spectral at different temperatures under 530 nm laser pumping; (b) lasing threshold as a function of temperature. Reproduced with permission from [16], H. Yang, et al., Transfer printing stacked nanomembrane lasers on silicon. *Nat. Photonics* 25, 658 **(2012)**. © 2012, Macmillan Publishers Limited.

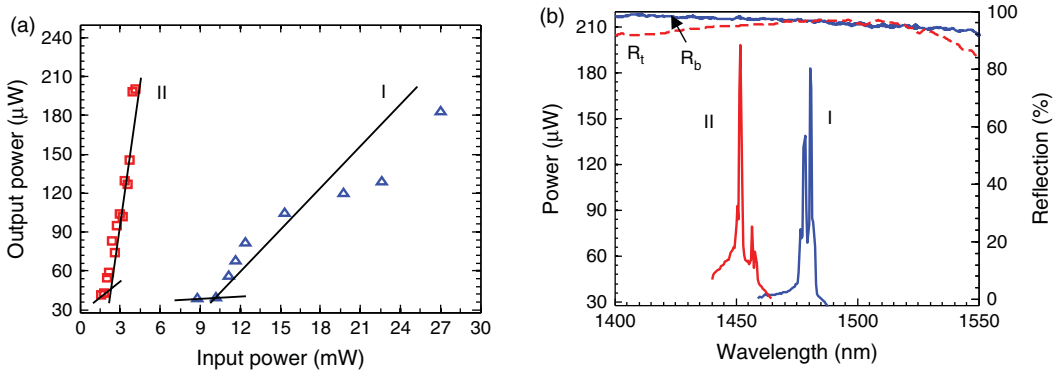

Fig. 14. (a) L–L plot (light output for different pump powers) at $T = 15$ K under 532 nm (I) and 980 nm (II) lasers pumping. (b) The corresponding lasing spectra and the measured reflections of top and bottom MRs.

(with 50% duty cycle). Shown in Figure 12(a) is the L–L plot (light output for different pump powers) and the corresponding spectral linewidths measured at $T = 50$K. The threshold pump power is ~ 8 mW, or 0.32 KW/cm^2. The measured spectral linewidths reduce from 30 nm below threshold to 0.6–0.8 nm above threshold. The measured spectral outputs are shown in Figure 12(b), for pump powers below, at, and above thresholds (points (i, ii, iii, iv) at L–L curve). The lasing spectral linewidth is ~ 8 Å, which is limited by the measurable resolution of monochrometer. The relative peak location shift shown in Figure 12(b) from bias levels (ii) and (iii, iv) is mostly related to mode hopping and temperature rise inside the active region at higher pump power levels.

This MR-VCSEL LT device was also characterized at different temperatures up to 120 K. Figure 13(a) shows the normalized lasing spectra (arbitrary units, a.u.) above the threshold at $T = 15$ K, 50 K, 70 K, 90 K, 120 K. The lasing peak red shifts as T increases and multimode lasing for most T cases at a rate ($d\lambda_c$/dT) close to the simulated 0.088 nm/K. There is a mode hopping occurred below and above the operation temperature of 80 K. As T rises higher than 125 K, there was no lasing any more, which is mainly limited by the MR reflector bandwidth except the QW emission becomes weak. The LT design cavity has three lasing wavelengths of 1448 nm (at 10 K), 1478 nm (at 50 K), and 1520 nm (at 120 K) which match well with the cavity resonances. Figure 13(b) shows the lasing threshold (L_{th}) as a function of T. L_{th} lineally increases with T, which matches the QW PL efficiency linearly decreases as T.

By improving cavity design and thermal engineered layers for improved thermal performance, we were able to drastically reduce the lasing threshold.[33] The measured L–L plots are shown in Figure 14(a) for a MR-VCSEL device under two types of c.w. pumping laser sources at $T = 15$K. By switching the pumping laser sources from 532 nm to 980 nm, the lasing thresholds reduce from 10 mW to 1.9 mW. The reduction of the lasing threshold is largely contributed to the significantly reduced thermal heating inside the lasing cavity. This is evident from the measured lasing spectral outputs, as shown in Figure 14(b), where the lasing spectral peaks shifts from 1482 nm (with 532 nm pump) to 1452 nm (with 980 nm pump). Such a large blue-shift in lasing wavelength is a strong evidence of much reduced heat dissipation. Further threshold reduction is possible with much improved cavity design and the incorporation of highly thermal conductive buffer layers. Also shown in Figure 14(b) is the measured reflection spectra of the top (R_t) and bottom (R_b) Si-MRs used for this MR-VCSEL.

We should point out that photonics and photonic crystals have many other applications and are under extensive investigation.[34–38] Here we just review and summarize the progress based on our own research group.

5. SUMMARY

In summary, we systematically reviewed the designs and characteristics of MR reflectors and MR-VCSEL cavity. Based on the careful design and analysis on the MR properties, the fabricated device shows the characteristics as it is expected by cavity design, which is confirmed by MR-VCSEL optical characteristic demonstrations. More design details should be considered in MR-based VCSEL than conventional DBR-VCSEL, such as larger reflection phase change and waveguide exaction in QW layer. The design procedure discussed in here is common for any kind of VCSEL using PC MRs. In addition, utilizing the advantage of transfer printing technique, the multi-layer membranes structure can have different types of interface control, so different material systems can be further integrated together with unlocked constraints in lattice mismatches and thermal mismatches, which is opening doors towards a wide range of applications in optoelectronic and photonic devices: MR-VCSEL can be further integrated with different functional photonic nanomembrane layers for modulation, routing, and 3D photonic/electronic integration; MR-VCSEL can be built and transferred onto any other flexible plastic substrates, making them attractive for applications in consumer electronics and biophotonics, etc.

Acknowledgments: The authors acknowledge help from MattiasHammar from KTH, Sweden. We also thank funding agencies and program directors for their instrumental support from US Air Force Office of Scientific Research (AFOSR, Dr. GernotPomrenke), and US Army Research Office (ARO, Dr. Michael Gerhold).

References and Notes

1. C. W. Wilmsen, H. Temkin, and L. A. Coldren, Vertical-cavity surface-emitting lasers, Design, Fabrication, Characterization, and Applications, Cambridge University Press, New York (**2001**), Vol. 24.
2. A. Karim, S. Bjorlin, J. Piprek, and J. E. Bowers, Long-wavelength vertical-cavity lasers and amplifiers. *Selected Topics in Quantum Electronics, IEEE Journal of* 6, 1244 (**2000**).
3. K. Iga, Surface-emitting laser-Its birth and generation of new optoelectronics field. *IEEE Journal of Selected Topics in Quantum Electronics* 6, 1201 (**2000**).
4. D. A. Louderback, H.-C. Lin, M. A. Fish, J. Cheng, and P. S. Guilfoyle, Three-dimensional integration of VCSEL-based optoelectronics. *Integrated Optoelectronic Devices* 2005, 50 (**2005**).
5. J. Witzens, A. Scherer, G. Pickrell, D. Louderback, and P. Guilfoyle, Monolithic integration of vertical-cavity surface-emitting lasers with in-plane waveguides. *Appl. Phys. Lett.* 86, 101105 (**2005**).
6. K. Iga, Vertical-cavity surface-emitting laser: its conception and evolution. *Japanese J. Appl. Phys.* 47, 1 (**2008**).
7. N. Nishiyama, C. Caneau, B. Hall, G. Guryanov, M. Hu, X. Liu, M.-J. Li, R. Bhat, and C. Zah, Long-wavelength vertical-cavity surface-emitting lasers on InP with lattice matched AlGaInAs-InP DBR grown by MOCVD. *Selected Topics in Quantum Electronics, IEEE Journal of* 11, 990 (**2005**).
8. C. F. R. Mateus, M. C. Y. Huang, Y. F. Deng, A. R. Neureuther, and C. J. Chang-Hasnain, Ultrabroadband mirror using low-index cladded subwavelength grating, *IEEE Photonics Technology Letters* 16, 518 (**2004**).
9. V. Lousse, W. Suh, O. Kilic, S. Kim, O. Solgaard, and S. H. Fan, Angular and polarization properties of a photonic crystal slab mirror. *Opt. Express* 12, 1575 (**2004**).
10. M. Shokooh-Saremi and R. Magnusson, Leaky-mode resonant reflectors with extreme bandwidths. *Opt. letters* 35, 1121 (**2010**).
11. Z. Qiang, H. Yang, S. Chuwongin, D. Zhao, Z. Ma, and W. Zhou, Design of Fano Broadband Reflectors on SOI. *Photonics Technology Letters, IEEE* 22, 110 (**2010**).
12. C. F. R. Mateus, M. C. Y. Huang, L. Chen, C. J. Chang-Hasnain, and Y. Suzuki, Broad-band mirror (1.12–1.62 mu m) using a subwavelength grating," *IEEE Photonics Technology Letters* 16, 1676 (**2004**).
13. M. C. Y. Huang, Y. Zhou, and C. J. Chang-Hasnain, A surface-emitting laser incorporating a high-index-contrast subwavelength grating (1, 119 (**2007**), *Nat. Photonics* 1, 297 (**2007**).
14. S. Boutami, B. Benbakir, J. L. Leclercq, and P. Viktorovitch, Compact and polarization controlled 1.55 mu m vertical-cavity surface-emitting laser using single-layer photonic crystal mirror. *Appl. Phys. Lett.* 91, 13 (**2007**).
15. C. Sciancalepore, B. B. Bakir, X. Letartre, J. Harduin, N. Olivier, C. Seassal, J. Fedeli, and P. Viktorovitch, CMOS-Compatible Ultra-Compact 1.55-μm Emitting VCSELs Using Double Photonic Crystal Mirrors. *Photonics Technology Letters, IEEE* 24, 455 (**2012**).
16. H. Yang, D. Zhao, S. Chuwongin, J.-H. Seo, W. Yang, Y. Shuai, J. Berggren, M. Hammar, Z. Ma, and W. Zhou, Transfer printing stacked nanomembrane lasers on silicon. *Nat. Photonics* 25, 658 (**2012**).
17. D. Y. Zhao, Z. Q. Ma, and W. D. Zhou, Field penetrations in photonic crystal fano reflectors. *Opt. Express* 18, 14152 (**2010**).
18. J. Kim, L. Chrostowski, E. Bisaillon, and D. Plant, DBR, Subwavelength grating, and Photonic crystal slab Fabry-Perot cavity design using phase analysis by FDTD. *Opt. Express* 15, 10330 (**2007**).
19. D. I. Babic and S. W. Corzine, Analytic expressions for the reflection delay, penetration depth, and absorptance of quarter-wave dielectric mirrors. *IEEE Journal of Quantum Electronics* 28, 514 (**1992**).
20. C. Sauvan, J. Hugonin, and P. Lalanne, Difference between penetration and damping lengths in photonic crystal mirrors. *Appl. Phys. Lett.* 95, 211101 (**2009**).
21. D. Zhao, H. Yang, S. Chuwongin, J. H. Seo, Z. Ma, and W. Zhou, Design of photonic crystal membrane reflector based VCSELs. *IEEE Photonics Journal* 4, 2169 (**2012**).
22. Y. C. Wang and S. S. Li, Design of a two-dimensional square mesh metal grating coupler for a miniband transport GaAs quantum-well infrared photodetector. *J. Appl. Phys.* 75, 582 (**1994**).
23. S. H. Fan and J. D. Joannopoulos, Analysis of guided resonances in photonic crystal slabs. *Phys. Rev. B* 65, 235112 (**2002**).
24. R. Magnusson and M. Shokooh-Saremi, Physical basis for wideband resonant reflectors. *Opt. Express* 16, 3456 (**2008**).
25. V. Karagodsky, F. G. Sedgwick, and C. J. Chang-Hasnain, Theoretical analysis of subwavelength high contrast grating reflectors. *Opt. Express* 18, 16973 (**2010**).
26. T. Sang, L. Wang, S. Y. Ji, Y. Q. Ji, H. Chen, and Z. S. Wang, Systematic study of the mirror effect in a poly-Si subwavelength periodic membrane. *Journal of the Optical Society of America A-Optics Image Science and Vision,* 26, 559 (**2009**).
27. H. Yang, S. Chuwongin, Z. Qiang, L. Chen, H. Pang, Z. Ma, and W. Zhou, Resonance control of membrane reflectors with effective index engineering. *Appl. Phys. Lett.* 95, 023110 (**2009**).
28. Z. X. Qiang, H. J. Yang, S. Chuwongin, D. Y. Zhao, Z. Q. Ma, and W. D. Zhou, Design of Fano Broadband Reflectors on SOI. *IEEE Photonics Technology Letters* 22, 1108 (**2010**).
29. H. J. Yang, D. Y. Zhao, J. H. Seo, S. Chuwongin, S. Kim, J. A. Rogers, Z. Q. Ma, and W. D. Zhou, Broadband Membrane Reflectors on Glass. *IEEE Photonics Technology Letters* 24, 476 (**2012**).
30. S. Boutami, B. B. Bakir, H. Hattori, X. Letartre, J. L. Leclercq, P. Rojo-Romeo, M. Garrigues, C. Seassal, and P. Viktorovitch, Broadband and compact 2-D photonic crystal reflectors with controllable polarization dependence. *Photonics Technology Letters, IEEE* 18, 835 (**2006**).
31. L. Coldren and S. Corzine, Diode lasers and photonic integrated circuits, Wiley, New York (**1995**).
32. A. F. Oskooi, D. Roundy, M. Ibanescu, P. Bermel, J. Joannopoulos, and S. G. Johnson, MEEP: A flexible free-software package for electromagnetic simulations by the FDTD method. *Comput. Phys. Commun.* 181, 687 (**2010**).
33. D. Zhao, S. Chuwongin, H. Yang, J. H. Seo, J. Berggren, M. Hammar, Z. Ma, and W. Zhou, Transfer printed photonic crystal nanomembrane lasers on silicon with low optical pumping threshold (post deadline paper), *2012 IEEE 9th International Conference on Group IV Photonics (GFP)*, San Diego, CA (**2012**), pp. 1–3.
34. S. Dhara and P. K. Giri, ZnO Nanowire Heterostructures: Intriguing Photophysics and Emerging Applications. *Rev. Nanosci. Nanotechnol.* 2, 147 (**2013**).
35. H. Y. Zhang, Y. H. Chen, and Z. G. Wang, Investigation of wetting layers in inas/gaas self-assembled nanostructures with reflectance difference spectroscopy. *Rev. Nanosci. Nanotechnol.* 1, 200 (**2012**).
36. R. Shabani and H. J. Cho, Nanomaterials in actuators-a review. *Rev. Nanosci. Nanotechnol.* 1, 85 (**2012**).
37. K. Vajravelu and K. V. Prasad, Natural and mixed convection heat transfer in nanofluids. *Rev. Nanosci. Nanotechnol.* 1, 142 (**2012**).
38. S. Tafur and M. N. Leuenberger, Spontaneous creation of photonic states in quantum dots, *Rev. Nanosci. Nanotechnol.* 1, 152 (**2012**).